frontiers in Physics

ORIGINAL RESEARCH
published: 10 March 2021
doi: 10.3389/fphy.2021.642302

Simultaneous Two-Photon Fluorescence Microscopy of NADH and FAD Using Pixel-to-Pixel Wavelength-Switching

Yifan Qin[1]* *and Yuanqin Xia*[2]*

[1]National Key Laboratory of Science and Technology on Tunable Laser, Harbin Institute of Technology, Harbin, China, [2]Center for Advanced Laser Technology, Hebei University of Technology, Tianjin, China

OPEN ACCESS

Edited by:
Ming Lei,
College of Science, Xi'an Jiaotong University, China

Reviewed by:
Shaowei Wang,
National University of Singapore, Singapore
Yang Yanlong,
State Key Laboratory of Transient Optics and Photonics, China

***Correspondence:**
Yifan Qin
qinyifanhit@gmail.com
Yuanqin Xia
xiayq@hebut.edu.cn

Specialty section:
This article was submitted to Optics and Photonics, a section of the journal Frontiers in Physics

Received: 15 December 2020
Accepted: 11 January 2021
Published: 10 March 2021

Citation:
Qin Y and Xia Y (2021) Simultaneous Two-Photon Fluorescence Microscopy of NADH and FAD Using Pixel-to-Pixel Wavelength-Switching. Front. Phys. 9:642302. doi: 10.3389/fphy.2021.642302

Two-photon fluorescence (TPF) microscopy of intrinsic fluorophores provides physiological and pathological information from biological tissues. Reduced nicotinamide adenine dinucleotide (NADH) and flavin adenine dinucleotide (FAD) are two endogenous fluorescent coenzymes existing on the intracellular scale. Autofluorescence images of NADH and FAD have been applied to noninvasively record changes during metabolism, according to their distributions and concentrations. However, the widely used sequential (non-simultaneous) excitation scheme results in artifacts caused by sample motion or laser power fluctuation. The single-wavelength illumination scheme suffers from low excitation efficiency and spectral bleed-through. In this paper, we demonstrate a new imaging system simultaneously capturing autofluorescence images from NADH and FAD, with high excitation efficiency and negligible spectral bleed-through. Two temporally multiplexed and spatially overlapped excitation beams were achieved with fast-switching light paths based on an electro-optic modulator. The switching beams were centered at 750 and 860 nm, enabling independent excitations of NADH and FAD. Autofluorescence images of NADH and FAD were acquired at the wavelength ranges of 415–455 nm and 500–550 nm, respectively. The electro-optic modulator was synchronized with the pixel clock from the microscope, achieving pixel-to-pixel wavelength-switching. The capability of the system was demonstrated by performing TPF imaging of freshly excised mouse colon tissues. The microenvironment of the colon wall was depicted by the distributions of colonocytes, goblet cells, and crypts of Lieberkühn, and the relative concentrations of NADH and FAD were estimated. The experimental results show that the system can effectively perform simultaneous imaging of NADH and FAD, and is considered a promising tool for investigations into metabolism-associated processes and diseases.

Keywords: nonlinear optical microscopy, label-free microscopy, NADH, FAD, two-photon fluorescence

INTRODUCTION

Two-photon fluorescence (TPF) microscopy has been proven to be a powerful technique for imaging in biological tissues [1]. In TPF, the emission intensity depends quadratically on the excitation intensity, which minimizes the signal gained out of the sample volume [2]. TPF microscopy has submicron three-dimensional spatial resolution, high signal-to-noize ratio, weak out-of-focus photobleaching, and good penetration ability, which are significant for biomedical applications. Meanwhile, TPF microscopy is a label-free technique because the existence of endogenous fluorophores in biological tissues eliminates the need for exogenous biomarkers for imaging.

Reduced nicotinamide adenine dinucleotide (NADH) and flavin adenine dinucleotide (FAD) are metabolic coenzymes, which are also the most widely used endogenous fluorophores [3, 4]. During metabolism, enzymes bind to NADH and FAD, and their relative concentrations and distributions change at the same time. TPF imaging of NADH and FAD enables noninvasively monitoring of metabolism-related physiological and pathological processes, such as cell differentiation, cancer development. One imaging scheme is sequential (non-simultaneous) excitation, which switches between two wavelengths (e.g., 755 and 860 nm) by using a tunable laser [5–7]. The advantage is that autofluorescence signals of NADH and FAD can be completely separated, and misinterpretation can be avoided during analysis. However, it suffers from low acquisition speed and artifacts from sample motion or laser power fluctuation when tuning between two wavelengths. Another scheme using single-wavelength (e.g., 800 nm) excitation can excite NADH and FAD simultaneously at the cost of unavoidable spectral bleed-through (SBT) and low excitation efficiency [8].

To overcome the shortages of the aforementioned two schemes, we demonstrate a novel TPF microscopy capable of exciting NADH and FAD simultaneously by using pixel-to-pixel wavelength-switching. The concept was proposed for nonlinear optical microscopy in our previous works [9, 10]. During pixel-to-pixel wavelength-switching, two temporally multiplexed excitation beams, centered at 750 and 860 nm, are achieved by using an electro-optic modulator (EOM). Since the EOM is synchronized with the pixel clock, the wavelengths and pixels switch simultaneously. The major advantages of the imaging system are as follows.

- Simultaneous excitations of NADH and FAD ensure high acquisition speed and eliminate possible artifacts from sample motion or laser power fluctuation.
- SBT is negligible and excitation efficiency is high because of the independent excitations and separated detections.
- The pixel-to-pixel wavelength-switching strategy doesn't require any complex demultiplexing algorithm to collect signal or internal modification to commercial microscopes (e.g., FV1000, Olympus, Japan).

We will describe the system construction step by step, and demonstrate the capability of the system by performing simultaneous TPF imaging in NADH and FAD solutions as well as in freshly excised mouse colon tissues.

EXPERIMENTAL SETUP

Figure 1A shows the experimental setup. The excitation source for the simultaneous TPF microscopy of NADH and FAD is a broadband (>100-nm spectral bandwidth) mode-locked Ti: Sapphire laser, which generates femtosecond pulses with ~80-MHz repetition rate. The laser beam is delivered to a liquid-crystal spatial light modulator (SLM, SLM-640-D-VN, CRi, United States)-based pulse shaper with a 4*f* configuration. The laser beam is dispersed by a grating onto a concave mirror and focused on an SLM placed at the Fourier plane. By setting the mask of the SLM, the laser beam is tailored to a double-peak spectrum, which is centered at 750 and 860 nm. These wavelengths are selected according to the cross-sections of NADH and FAD (**Figure 1B**). The cross-section spectra indicate that the 860-nm wavelength can only excite FAD, while the 750-nm wavelength can excite both substances.

A long-pass dichroic mirror (DM1, DMLP805R, Thorlabs, United States) splits the laser beam into two arms, i.e., the transmitted 860-nm arm (shown in red) and the reflected 750-nm arm (shown in blue). Both arms are initially p-polarized. In the 860-nm arm, a polarizing beam splitter (PBS1, PBS102, Thorlabs, United States) and a half-wave plate (HWP1, WPH05M-850, Thorlabs, United States) are combined to adjust the optical power. Fine-tuning the relative position of lenses L1 and L2 (AD408-B, LBTEK, China, $f_{L1} = f_{L2} = 100$ mm) along the optical axis can compensate for the axial displacement between the two arms derived from chromatic aberration [11]. In the 750-nm arm, a polarizing beam splitter (PBS2, PBS102, Thorlabs, United States) and a half-wave plate (HWP2, WPH05M-780, Thorlabs, United States) are paired to rotate the polarization by 90° (to s-polarized) and adjust the optical power. A long-pass dichroic mirror (DM2, DMLP805R, Thorlabs, United States) recombines the two arms. Spatial synchronization of the two arms is achieved by using the same method described in [10]. A quarter-wave plate (QWP, WPQ05M-808, Thorlabs, United States) and an EOM (EO-AM-NR-C1, Thorlabs, United States) are located after DM2. The modulation signal of the EOM is from a function generator (SDG1032X, Siglent, China). When applying a $4/\lambda$ voltage, the EOM and QWP work as a half-wave plate, which rotates the polarizations of incoming beams by 90°. When applying a $-4/\lambda$ voltage, the polarizations will stay the same. A polarizing beam splitter (PBS3, PBS102, Thorlabs, United States) located after the EOM removes s-polarized components. The voltages applied to the EOM rapidly switch between $\pm 4/\lambda$ (the frequency is 125 kHz, the duty cycle is 50%). Thus the 860- and 750-nm beams are spatially overlapped and temporally multiplexed. Proper dispersion management are performed for both arms. All the optical elements mentioned above comprise the EOM-based fast-switching light paths.

A dual-axis galvanometer-scanner (GVS002, Thorlabs, United States) scans the beams at the focal plane of a scan lens (AC254-045-B, Thorlabs, $f_{SL} = 45$ mm). The beams are

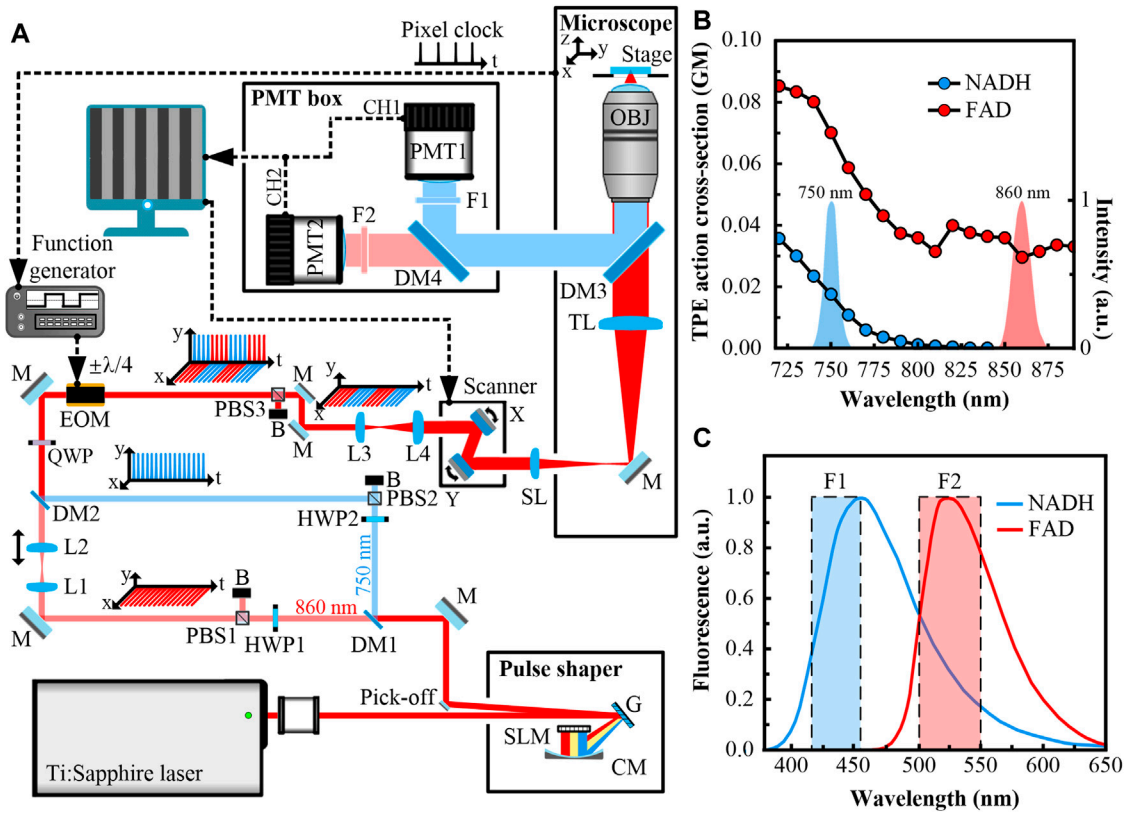

FIGURE 1 | (A) Experimental setup of the simultaneous two-photon fluorescence (TPF) microscopy of NADH and FAD. The laser beams are mainly shown in red, except that the 750-nm beam is shown in blue. Signals collected by CH1 are indicated in blue, and those collected by CH2 are indicated in red. The electrical paths are depicted in dashed black lines. HWP1, HWP2, half-wave plates; SLM, spatial light modulator; G, grating; CM, concave mirror; M, mirror; DM1, DM2, DM3, DM4, long pass dichroic mirrors; PBS1, PBS2, PBS3, polarizing beam splitters; B, blocker; L1, L2, L3, L4, lenses; QWP, quarter-wave plate; EOM, electro-optic modulator; SL, scan lens; TL, tube lens; OBJ, objective; F1, F2, bandpass filters; PMT1, PMT2, photomultiplier tubes. This figure is not to scale. **(B)** Spectra of shaped pulses overlaid with two-photon excitation (TPE) action cross-section spectra of reduced nicotinamide adenine dinucleotide (NADH) and flavin adenine dinucleotide (FAD). The cross-section is shown in GM unit (1 GM = 10^{-50} $cm^4 \cdot s \cdot photon^{-1} \cdot molecule^{-1}$). The spectra show that both substances can be excited at 750 nm, but only FAD can be excited at 860 nm. **(C)** The emission spectra of NADH and FAD. The filters are chosen to collect the emissions of NADH and FAD with minimum crosstalk.

focused by the scan lens, and delivered into a modified inverted microscope (IX71, Olympus, Japan). The scan lens, a tube lens (f_{TL} = 180 mm), and lenses L3 and L4 (AD406-B, AD408-B, LBTEK, China, f_{L3} = 50 mm, f_{L4} = 100 mm, placed before the scanner) expand the beams to fit the back-aperture of a 20× 1.00NA water immersion objective lens (XLUMPLFLN, Olympus, Japan). The scan lens and the tube lens constitute a 4*f* optical system, imaging the middle plane of the scanner to the entrance pupil of the objective. The objective collects and focuses the incoming beams into samples, which sit on a three-dimensional motorized stage.

Autofluorescence from samples is collected by the objective in the epi-direction, filtered from the fundamental beams by a long-pass dichroic mirror (DM3, FF660-Di02, Semrock, United States). Another long-pass dichroic mirror (DM4, FF470-Di01, Semrock, United States) is combined with two bandpass filters (F1, F2, FF02-435/40, FF03-525/50, Semrock, United States) to separate autofluorescence at different emission bands and minimize SBT (**Figure 1C**). Signals are detected by two channels (CH1, CH2), which are equipped with two photomultiplier tubes (PMT1, PMT2, R6357, Hamamatsu, Japan). The achieved wavelength ranges for CH1 and CH2 are 415–455 nm and 500–550 nm, respectively. As shown in **Figure 1C**, CH1 only collects autofluorescence from NADH, while CH2 collects autofluorescence from both NADH and FAD. However, using the excitation/detection combination of 860/500–550 nm ensures that only CH2 gains autofluorescence from FAD. Imaging software simultaneously drives the scanner and restores images from different detection channels with noises subtracted.

Meanwhile, the pixel clock from the microscope with a 4-μs period serves as the external trigger for the function generator (**Figure 2A**). The generated pulse train has an 8-μs period with a 50% duty cycle (**Figure 2B**). As mentioned above, the EOM is modulated by the function generator. Fine-tuning the time-delay of the modulation pulse train will ensure that only the 860- or 750-nm arm is turned on in each pixel time. This method is called pixel-to-pixel wavelength-switching. **Figure 2C** shows a stripe pattern image obtained by this method. The signal was derived from FAD in

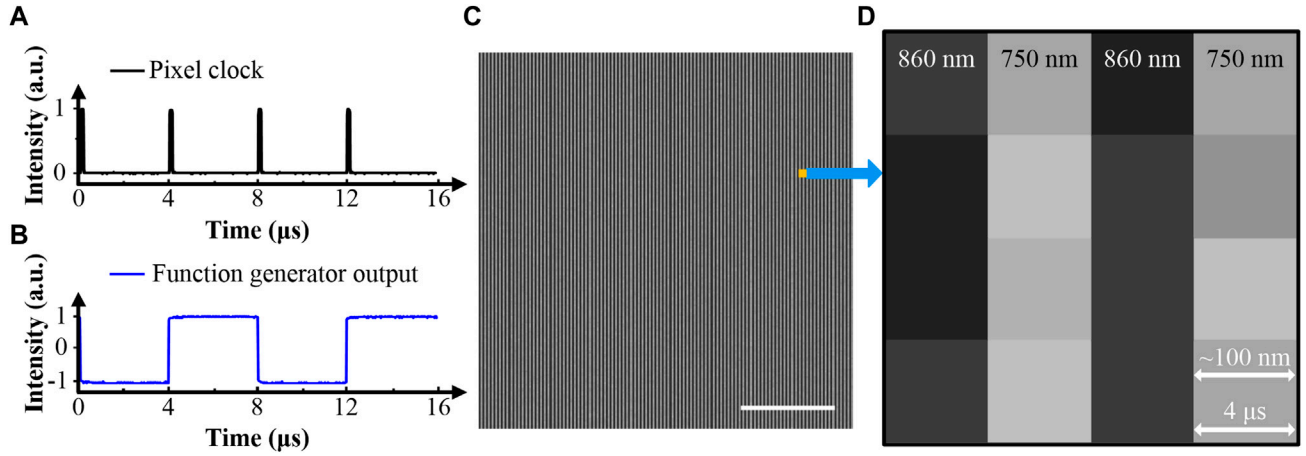

FIGURE 2 | (A) The pixel clock from the microscope. **(B)** The pulse train from the function generator. **(C)** Demonstration of TPF imaging using pixel-to-pixel wavelength-switching, 4 μs/pixel, 200×200 pixels. The stripe pattern image is acquired from FAD in a buffered solution. **(D)** Zoomed-in view of **(C)**, 4×4 pixels. Signals gained with different excitation wavelengths are displayed in different columns. The scale bar is 5 μm.

solution, and only CH2 was turned on. **Figure 2D** is a zoomed-in view of **Figure 2C**. It shows the odd columns corresponding to the 860-nm excitation appear dark, and the even columns corresponding to the 750-nm excitation are bright. The results are consistent with the cross-section spectrum of FAD shown in **Figure 1B**. The stability of the imaging system is mainly determined by the performance of pixel-to-pixel wavelength-switching. Recording the contrast between bright and dark columns in stripe pattern images provides a direct way to evaluate the system stability. We acquired three stacks of stripe pattern images from the FAD solution. During the acquisition of a stack, the excitation beams kept scanning the same region of interest (ROI). Five images were captured with 15-s intervals. The three stacks had 30-min intervals. The excitation beams were blocked between acquisitions of different stacks. These images show that the fluctuation of the contrast between bright and dark columns is within ±1%. The system is considered stable in both short- and long-term runs. Note that all electrical devices equipped in the setup are commercially available. Wiring can be operated by researchers without plentiful knowledge of electrical engineering.

RESULTS AND DISCUSSION

We first demonstrate the capability of the imaging system in NADH and FAD solutions. The NADH and FAD solutions used in the experiments had the same concentrations. Both CH1 and CH2 were turned on. **Figure 3A** shows the TPF images of NADH and FAD solutions, corresponding to different excitation/detection combinations. When imaging the NADH solution, both CH1 (415–455 nm) and CH2 (500–550 nm) channels can gain signal with 750-nm excitation, but all pixels appear dark in images acquired with 860-nm excitation. **Figure 3B** depicts the average intensities of these images, which are consistent with the cross-section spectrum of NADH (**Figure 1B**). Note that all four images of NADH were simultaneously acquired because of the utilization of pixel-to-pixel wavelength-switching. When imaging the FAD solution, CH2 can gain signal at both excitation wavelengths, but pixels appear dark in images obtained in CH1. **Figure 3C** shows the average intensities of these images. The results show that the bandpass filter of CH1 can effectively avoid SBT from CH2. Note that all four images of FAD were simultaneously acquired. If a mixture of both NADH and FAD is applied as the specimen, the excitation/detection combination of 750/500–550 nm is not suitable for imaging NADH or FAD anymore, because of severe SBT. The final excitation/detection combinations for NADH and FAD are as follows.

- NADH: 750/415–455 nm (excitation/detection), marked by * in **Figure 3A.**
- FAD: 860/500–550 nm (excitation/detection), marked by † in **Figure 3A.**

The capability of the imaging system is then demonstrated by using freshly excised mouse colon tissues. The mouse was sacrificed by applying cervical dislocation. The colon was removed immediately, and a segment was obtained. The segment was dissected longitudinally and kept in chilled phosphate-buffered saline until imaging. The animal study was reviewed and approved by the Institutional Animal Care and Use Committee of Hebei University of Technology.

The murine gastrointestinal tract, along the proximal-distal axis, comprises the mouth, esophagus, stomach, small intestine, large intestine (including the cecum, colon, and rectum), and anus. The primary functions of the stomach along with the small intestine are enzymatic digestion and absorption of nutrients [12]. The cecum occupies a large proportion of the murine abdominal cavity. It ferments digesta and produces vitamins and fatty acids by bacteria [13]. The colon can be further divided into the proximal colon, mid colon, and distal colon. It is mainly responsible for reabsorbing electrolytes and dehydrating. The stool from the colon will be pushed out of the body through the rectum and anus [14]. The colonic wall

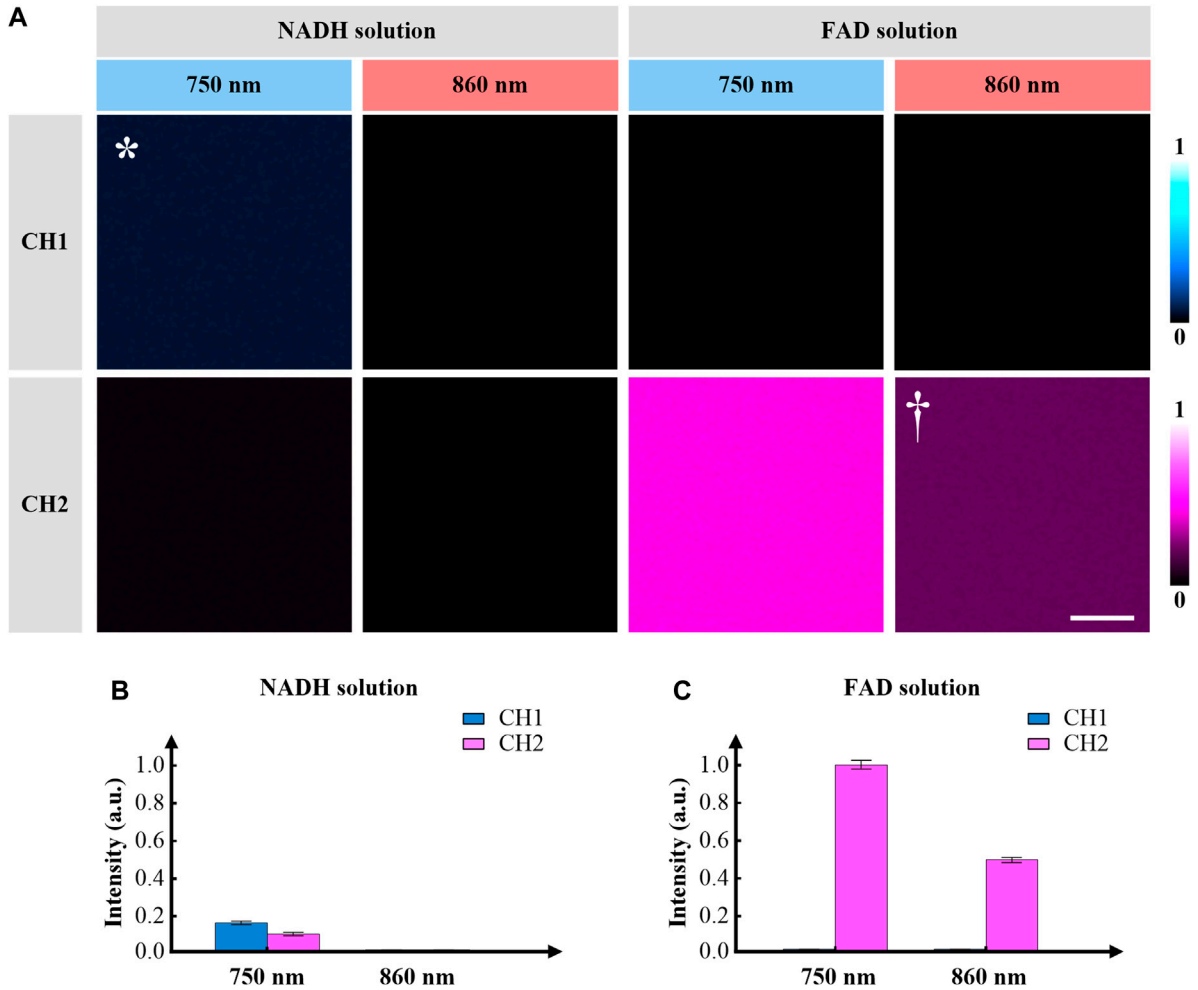

FIGURE 3 | (A) Representative TPF images of NADH and FAD solutions using pixel-to-pixel wavelength-switching, equivalent 8 μs/pixel, 100×100 pixels. The solutions are excited at 750 and 860 nm, and the signals are collected at the wavelength ranges of 415–455 nm (CH1) and 500–550 nm (CH2). The excitation/detection combinations of 750/415–455 nm and 860/500–550 nm are used to collect TPF images of NADH (marked by *) and FAD (marked by †), respectively. **(B)** Fluorescence intensities of different excitation/detection combinations, when imaging the NADH solution. **(C)** Fluorescence intensities of different excitation/detection combinations, when imaging the FAD solution. Error bars represent standard error. The scale bar is 5 μm.

consists of four tissue layers, which are the mucosa, submucosa, muscular tunic, and serosa [15]. The mucosa consists of closely packed crypts of Lieberkühn and intercryptal epithelial surfaces. The predominant cells in the mucosa are columnar absorptive colonocytes and mucus-secreting goblet cells. Investigations into colonic diseases, e.g., inflammatory and cancer, can be performed by analyzing autofluorescence derived from NADH and FAD in the cytoplasm of these cells.

Figure 4 shows the simultaneously acquired TPF images of NADH and FAD into mouse colonic mucosa. The pixel time was adjusted to improve signal level. **Figure 4A** is an autofluorescence image of NADH, which shows that the colonic mucosa comprises a prominent population of colonocytes (identified by the fluorescent cytoplasm) and the crypts of Lieberkühn. The cells indicated by the white arrows are probably goblet cells, whose mucus is usually nonfluorescent. The white oval marks a crypt of Lieberkühn. The image confirms that the system reveals the microenvironment of the mouse colonic mucosa. **Figure 4B** is an autofluorescence image of FAD in the same ROI. **Figures 4A,B** were obtained simultaneously at the depth of 15 μm. According to the similar morphological features and boundaries shown in **Figures 4A,B**, the axial displacement between the 750- and 860-nm arms, which originated from chromatic aberration, was negligible. **Figures 4C,D** are autofluorescence images of NADH and FAD simultaneously obtained at the depth of 20 μm. In **Figures 4A,C,** the white ovals outline the same crypt, and the white arrows denote the same cells (probably goblet cells). It indicates that the focal plane moves in the axial direction without tilt.

It is known that the autofluorescence intensity is proportional to the concentration of substances [16]. In our experiment, NADH has a smaller cross-section than FAD, but the fluorescence is stronger in NADH images (**Figure 4**). We consider that FAD in mouse colonic mucosa is relatively sparse comparing with NADH, which is consistent with

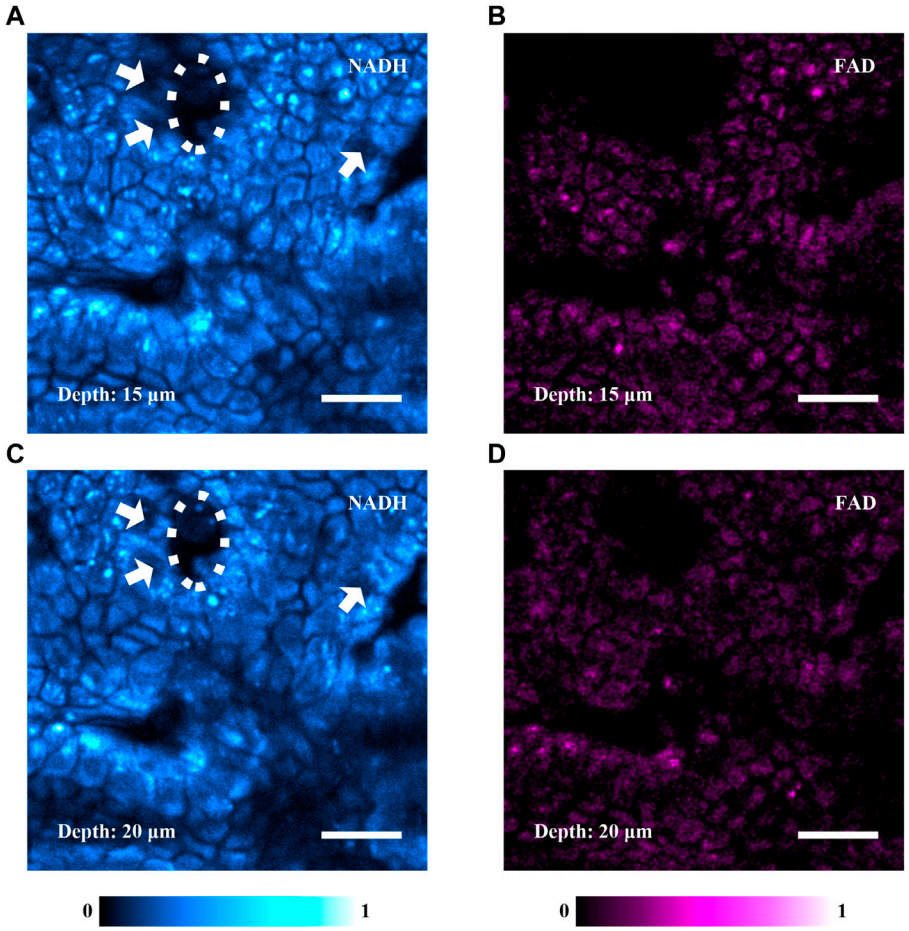

FIGURE 4 | Simultaneously acquired TPF images of NADH and FAD in mouse colonic mucosa, equivalent 20 μs/pixel, 512×512 pixels. **(A)** A TPF image of NADH acquired at the depth of 15 μm into the colonic mucosa. It shows that the colonic mucosa predominantly comprises colonocytes and crypts of Lieberkühn. The white arrows indicate a few cells, which are probably goblet cells. The white oval denotes a crypt. **(B)** A TPF image of FAD simultaneously acquired at the same region of **(A)** in the colonic mucosa. **(C,D)** TPF images of NADH and FAD simultaneously acquired at the depth of 20 μm. The white arrows in **(C)** indicate the same cells in **(A)**. The white oval in **(C)** denotes the same crypt in **(A)**. The scale bars are 20 μm.

previously published data [17, 18]. The experimental results show that the system can effectively perform simultaneous imaging of NADH and FAD, and metabolism-related quantitative analysis may be carried out with sufficient prior knowledge of tissues. Adding photon-counting modules will enable the imaging system to perform two-photon fluorescence lifetime imaging microscopy (FLIM) for studying complicated pathological processes.

Although the pixel size is set to ~100 nm in the experiments, different values can be selected upon the intensity point spread function (IPSF), which describes the spatial intensity near the focus. Since the intensity of TPF is proportional to the square of the excitation intensity, $IPSF^2$ can define the optical resolution. According to the $IPSF^2$ formulas in [1], the lateral resolutions of our system are theoretically 290 and 330 nm with 750- and 860-nm excitations, respectively. With pixel sizes smaller than 145 nm, two adjacent pixels will fall in the same resolution volume in the focal plane, ensuring high imaging performance. In practice, it's usual to find that lateral resolution may reduce to >600 nm with similar configurations [2]. Thus, a pixel size up to 300 nm will still be able to avoid mismatches between NADH and FAD images.

CONCLUSION

Simultaneous TPF microscopy of NADH and FAD is achieved by using pixel-to-pixel wavelength-switching. It provides negligible SBT and high excitation efficiency using simultaneous excitations of NADH and FAD, without the need to modify commercial microscopes. What's more, comprehensive knowledge in the field of electrical engineering is not necessary to set up the imaging system. Autofluorescence images of mouse colonic mucosa reveal the distributions and the relative concentrations of NADH and FAD, which provides a promising tool for investigations into metabolism-associated diseases in excised tissues. Note that the excitation intensities of NADH and FAD can be controlled independently with each other. Even though FAD is sparse in some tissues, its signal

level can still be comparable with that of NADH by properly increasing the average power of the 860-nm arm. Although only *in vitro* experiments are demonstrated, the imaging system has the potential to perform *in vivo* investigations. The frame rate is restricted to the order of seconds by using a galvanometer-scanner [19], which seems inadaptable for many *in vivo* applications [20]. However, the size of an ROI (e.g., accumulation of mitochondria) is usually around 10×10 pixels in a standard image of 512×512 pixels. By using pixel-to-pixel wavelength-switching, the acquisition time to obtain simultaneous local images of NADH and FAD in an ROI is on the order of one hundred microseconds, which is sufficiently short to track cellular dynamics of *in vivo* metabolic activity without image blur.

DATA AVAILABILITY STATEMENT

The original contributions presented in the study are included in the article/Supplementary Material, further inquiries can be directed to the corresponding authors.

ETHICS STATEMENT

The animal study was reviewed and approved by the Institutional Animal Care and Use Committee of Hebei University of Technology.

AUTHOR CONTRIBUTIONS

Conception, YQ and YX; investigation, YQ; design, YQ; software, YQ; data acquisition, YQ; analysis, YQ; original draft, YQ; review and editing, YQ, YX; supervision, YX; project administration, YX; funding acquisition, YX. All authors approved the submitted version.

FUNDING

This research was funded by the National Natural Science Foundation of China, grant numbers 61975050, 61675057.

REFERENCES

1. Zipfel WR, Williams RM, Webb WW. Nonlinear magic: multiphoton microscopy in the biosciences. *Nat Biotechnol* (2003) 21:1369–77. doi:10.1038/nbt899
2. Lefort C. A review of biomedical multiphoton microscopy and its laser sources. *J Phys D Appl Phys* (2017) 50:423001. doi:10.1088/1361-6463/aa8050
3. Denk W, Strickler JH, Webb WW. Two-photon laser scanning fluorescence microscopy. *Science* (1990) 248:73–76. doi:10.1126/science.2321027
4. Heikal AA. Intracellular coenzymes as natural biomarkers for metabolic activities and mitochondrial anomalies. *Biomark. Med* (2010) 4:241–263. doi:10.2217/BMM.10.1
5. Skala MC, Riching KM, Gendron-Fitzpatrick A, Eickhoff J, Eliceiri KW, White JG., et al. *In vivo* multiphoton microscopy of NADH and FAD redox states, fluorescence lifetimes, and cellular morphology in precancerous epithelia. *Proc Natl Acad Sci USA* (2007) 104:19494–9. doi:10.1073/pnas.0708425104
6. Quinn KP, Bellas E, Fourligas N, Lee K, Kaplan DL, Georgakoudi I. Characterization of metabolic changes associated with the functional development of 3D engineered tissues by non-invasive, dynamic measurement of individual cell redox ratios. *Biomaterials* (2012) 33:5341–8. doi:10.1016/j.biomaterials.2012.04.024
7. Varone A, Xylas J, Quinn KP, Pouli D, Sridharan G, McLaughlin-Drubin ME., et al. Endogenous two-photon fluorescence imaging elucidates metabolic changes related to enhanced glycolysis and glutamine consumption in precancerous epithelial tissues. *Cancer Res* (2014) 74:3067–75. doi:10.1158/0008-5472.can-13-2713
8. Huang S, Heikal AA, Webb WW. Two-photon fluorescence spectroscopy and microscopy of NAD(P)H and flavoprotein. *Biophys J* (2002) 82:2811–25. doi:10.1016/s0006-3495(02)75621-x
9. Wang S, Qin Y, Guo M, Zhang S, Xia Y. High speed 3D two-photon fluorescence microscopy by femtosecond laser pulses. *Proc. SPIE* (2017) 10605:106053J. doi:10.1117/12.2295704
10. Qin Y, Chen D, Xia Y. Real-time multidepth multiphoton microscopy using pixel-to-pixel focus-switching. *Appl Sci* (2020) 10:7173. doi:10.3390/app10207173
11. Filippi A, Dal Sasso E, Iop L, Armani A, Gintoli M, Sandri M., et al. Multimodal label-free *ex vivo* imaging using a dual-wavelength microscope with axial chromatic aberration compensation. *J Biomed Opt* (2018) 23:1–9. doi:10.1117/1.jbo.23.9.091403
12. Nishiyama K, Sugiyama M, Mukai T. Adhesion properties of lactic acid bacteria on intestinal mucin. *Microorganisms* (2016) 4:34. doi:10.3390/microorganisms4030034
13. Williams JM, Duckworth CA, Vowell K, Burkitt MD, Pritchard DM. Intestinal preparation techniques for histological analysis in the mouse. *Curr Protoc Mouse Biol* (2016) 6:148–68. doi:10.1002/cpmo.2
14. Nguyen TL, Vieira-Silva S, Liston A, Raes J. How informative is the mouse for human gut microbiota research? *Dis Model Mech* (2015) 8:1–16. doi:10.1242/dmm.017400
15. Hugenholtz F, de Vos WM. Mouse models for human intestinal microbiota research: a critical evaluation. *Cell Mol Life Sci* (2018) 75:149–60. doi:10.1007/s00018-017-2693-8
16. Qin Y, Li Q, Xia Y, Liu B, Zhang S. Construction and application of femtosecond laser two-photon fluorescence microscopy system. *J Harbin Inst Technol* (2015) 47:1–5. doi:10.11918/j.issn.0367-6234.2015.11.001
17. Ma N, Digman MA, Malacrida L, Gratton E. Measurements of absolute concentrations of NADH in cells using the phasor FLIM method. *Biomed Opt Express* (2016) 7:2441–52. doi:10.1364/boe.7.002441
18. Kimata S, Mochizuki D, Satoh J, Kitano K, Kanesaki Y, Takeda K., et al. Intracellular free flavin and its associated enzymes participate in oxygen and iron metabolism in *Amphibacillus xylanus* lacking a respiratory chain. *FEBS Open Bio* (2018) 8:947–61. doi:10.1002/2211-5463.12425
19. Deng Y, Qin Y, Zhang Z, Zhang Z, Xia Y. Simultaneous label-free two-photon fluorescence and second-harmonic generation microscopy for visualization of mouse pulmonary alveoli. *Proc SPIE* (2020) 11549:1154916. doi:10.1117/12.2573614
20. Goto A, Otomo K, Nemoto T. Real-time polarization-resolved imaging of living tissues based on two-photon excitation spinning-disk confocal microscopy. *Front Phys* (2019) 7:56. doi:10.3389/fphy.2019.00056

Conflict of Interest: The authors declare that the research was conducted in the absence of any commercial or financial relationships that could be construed as a potential conflict of interest.